ECS Transactions, 11 (4) 441-449 (2007)
10.1149/1.2779580 ©The Electrochemical Society

Electronic Properties of Adsorbates on $In_{0.37}Ga_{0.63}As(001)$-(2×4)

D. L. Winn, T. J. Grassman, and A. C. Kummel

Department of Chemistry and Biochemistry, University of California, San Diego, La Jolla, California 92093, USA

Molecular and electronic structures of In_2O and Ga_2O bonding to the As-rich $In_{0.37}Ga_{0.63}As(001)$-(2×4) surface were investigated using density functional theory (DFT) modeling. Calculated enthalpies of adsorption revealed that the bonding geometries of In_2O and Ga_2O on $In_{0.37}Ga_{0.63}As(001)$-(2×4) were essentially identical to those on GaAs(001)-(2×4). However, the calculated electronic structures resulting from the adsorbates/semiconductors systems exhibited subtle differences. Both oxides induced state density in the band gap consistent with Fermi level pinning on $In_{0.37}Ga_{0.63}As(001)$-(2×4) and GaAs(001)-(2×4). In addition, the state density worsened with increasing adsorbate coverage. However, a greater adsorbate density was required for the onset of Fermi level pinning for InGaAs than GaAs. This effect was attributed to reduction in band gap for $In_{0.37}Ga_{0.63}As(001)$-(2×4) *vs.* GaAs(001)-(2×4). Variations in the alloy structure of InGaAs (i.e. subsurface locations of In and Ga atoms) were found to play only a minor role on the resulting oxide adsorbate bonding geometries and electronic structures.

Introduction

InGaAs is a promising material for long wavelength optical communication devices (1). Several groups have attempted to construct InGaAs metal oxide semiconductor field effect transistor (MOSFET) devices (2, 3). Currently, InGaAs devices employ either GaAs or InP substrates. Increasing the In content raises the carrier mobilities of the alloy, but lattice matching limits InGaAs grown on GaAs to a very thin layer (~100 Å) of ~30% In content. While higher In content alloys can be grown on InP, InGaAs/GaAs is of technical interest due to the availability of large GaAs substrates and the ability to grow GaAs on Ge or GOI (Ge on insulator) wafers. Multiple studies have investigated oxides deposited on InGaAs in order to ascertain which oxide induces the least amount of states in the band gap region; these oxides include $Ga_2O_3(Gd_2O_3)$, Al_2O_3, and thermally oxidized AlAs (1-3). Although these studies have been able to demonstrate both working depletion (3) and enhancement mode (2) MOSFET devices, the electronic properties of these devices could be improved with an atomic understanding of the oxide/InGaAs interface.

In spite of the technological importance of InGaAs(001), only recently have experiments been performed to understand and characterize the surface at the atomic level. In order to characterize the clean surface, several groups have performed scanning tunneling microscopy (STM) studies to identify the different surface reconstructions of InGaAs(001). Although there are still disagreements about the exact surface

reconstructions, most groups agree that there are at least (2×4) and (n×3) surface reconstructions (4-6).

Very few computational papers have been published on InGaAs(001), (7-12) and none of this work has addressed oxide bonding on the InGaAs(001)-(2×4) surface. In this manuscript, DFT calculations will be presented of the clean $In_{0.37}Ga_{0.64}As(001)$-(2×4) surface along with calculations predicting the bonding geometries of In_2O and Ga_2O adsorbates. The 37% In content was chosen because it is close to the maximum In content for very thin InGaAs layers on GaAs.

Computational Techniques

$In_{0.37}Ga_{0.63}As(001)$-(2×4) was modeled using plane-wave (periodic boundary) DFT calculations. The calculations were performed using the Vienna *Ab-initio* Simulation Package (VASP) (13-16). The computational InGaAs surface slabs consisted of eight atomic layers with the bottom layer being terminated with H atoms. In order to preserve the bulk like properties of the system, the bottom three layers of the slab, along with the H atoms, were frozen in bulk position. Eleven layers of vacuum were used to avoid interactions between the top and the bottom of the slabs. The calculations were performed using the PW91 general gradient approximation exchange-correlation functional (17). Atoms were modeled using Vanderbilt ultrasoft pseudopotentials, as supplied by VASP (18, 19). A 4×2×1 Monkhorst-Pack (20) k-point sampling scheme was employed, which resulted in the generation of four irreducible k-points in the first Brillouin zone. The plane wave cut-off energy was set to 475 eV, and the slab was considered fully relaxed when the interatomic forces were all below 0.03 eV/Å. The error in these calculations is estimated to be ± 0.1 eV. A detailed discussion of how the ± 0.1 eV error value was estimated is presented elsewhere (21).

Results and Discussion

Clean $In_{0.37}Ga_{0.63}As(001)$-(2×4) surface

DFT calculations have been performed on numerous III-V semiconductors. However, when modeling alloy semiconductors, such as InGaAs, the procedure is slightly more complicated due to variability in the locations of the different species (e.g. In and Ga atoms). Figure 1(a) shows a ball and stick diagram of the clean InGaAs(001)-(2×4) surface. As atoms are depicted as orange circles and In or Ga atoms are depicted as black circles. An In concentration of 37% was used for this study, resulting in a slab that contained 11 In atoms and 19 Ga atoms.

The main complication in the placement of the In and Ga atoms is that although the placements can be random within the slab, the periodic boundary conditions will cause the formation of long-range order. In an effort to verify that this quasi-order will not affect the computational results, four different slabs were constructed with random placements of the Ga and In atoms [Fig. 1(b)-1(e)]. The four slabs had total energies of -280.23, -280.06, -280.75, and -280.48 eV. The span in energies results from differences in surface energy of the structures along with bulk energy differences most likely due to strain. The molecular beam epitaxially grown samples are expected to have a random

placement of In and Ga atoms in the bulk, with slightly higher In concentrations at the surface (22).

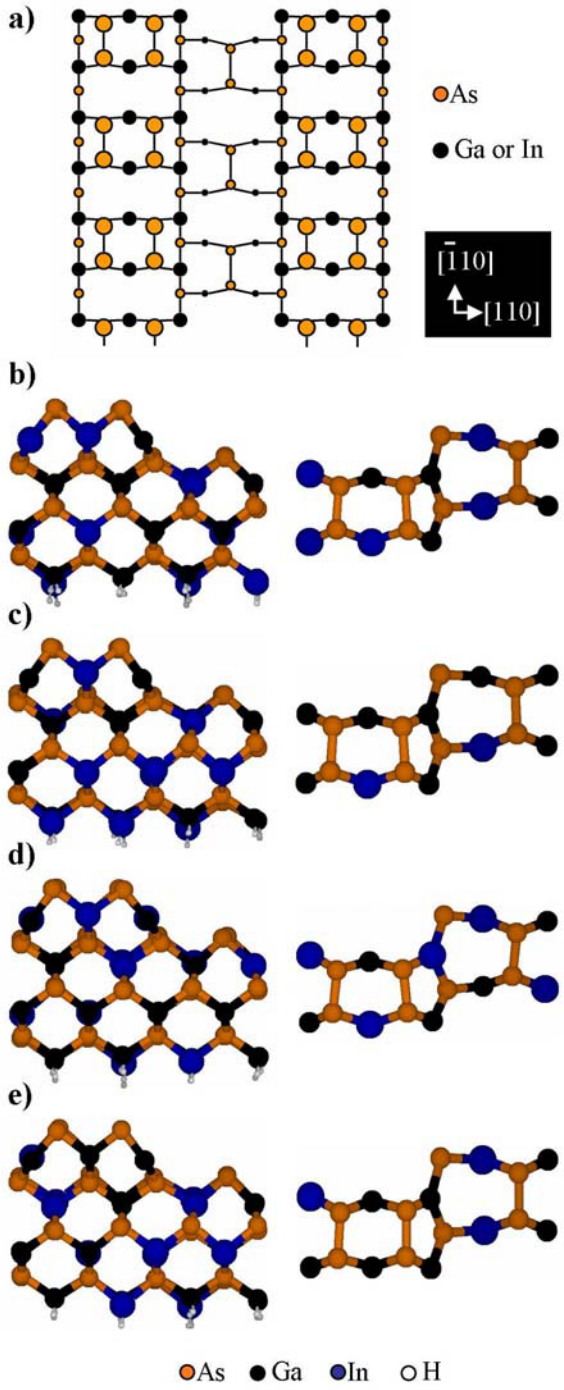

FIGURE 1. (a) Ball-and-stick diagram of the clean InGaAs(001)-(2×4) surface. Side and top-down views of (b) geometry 1, (c) geometry 2, (d) geometry 3, and (e) geometry 4.

Although the differences in total energy between the four slabs were not substantial, it was also important to verify that the In and Ga placements did not effect the electronic properties of the system. Figure 2 shows the calculated densities of states (DOS) of the four clean InGaAs geometries. From the plot, it can be seen that the electronic properties

of the slabs remain the same regardless of the placements of the In or the Ga atoms. Therefore, only one bonding geometry was chosen for subsequent calculations of the bonding of In_2O and Ga_2O molecules to the $In_{0.37}Ga_{0.63}As(001)$-(2×4) surface. Geometry (b) in Fig. 1 was chosen due to its even mixture of surface In and Ga atoms.

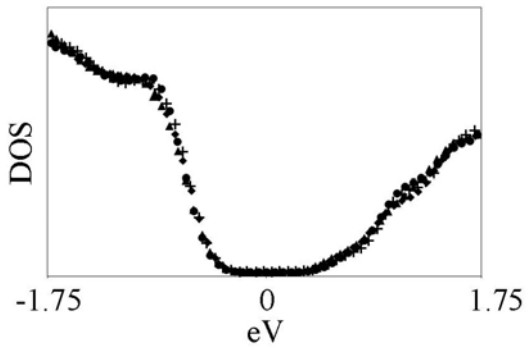

FIGURE 2. DOS of four different slabs with random In placements: geometry 1 (●), geometry 2 (▲), geometry 3 (+), and geometry 4 (♦). All of the DOS line up and possess no significant differences, therefore, the In placement does not effect the electronic properties of the slab.

In_2O and Ga_2O bonding to $In_{0.37}Ga_{0.63}As(001)$-(2×4)

The In_2O and Ga_2O bonding sites along with the enthalpies of adsorption are presented in Fig. 3. Winn *et al.* (23) performed a similar study of In_2O and Ga_2O bonding to the GaAs(001)-(2×4) surface; a summary of their findings, along with the findings in the current paper, are presented in Table 1. Although the computational methods vary slightly, the overall trends between the two systems are comparable.

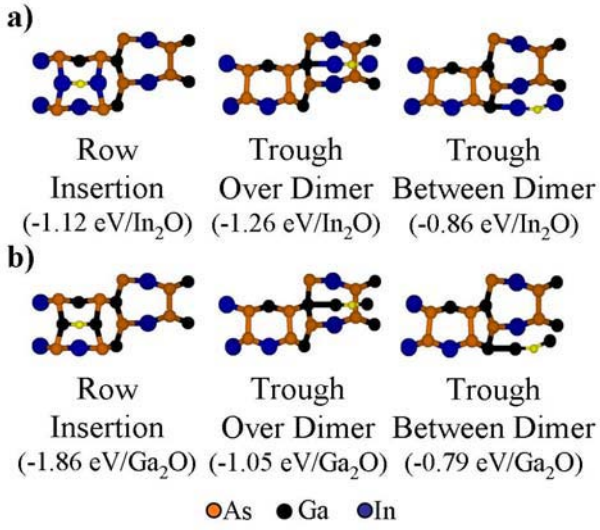

FIGURE 3. Top-down views of the (a) In_2O and (b) Ga_2O bonding sites on $In_{0.37}Ga_{0.63}As(001)$-(2×4).

TABLE I. Summary of the findings for In_2O and Ga_2O bonding to the GaAs(001)-(2×4) and $In_{0.37}Ga_{0.63}As$(001)-(2×4).

	GaAs (ΔH_{abs})	**$In_{0.37}Ga_{0.63}As$** (ΔH_{abs})
In_2O Half Coverage Insertion	-1.18 eV/In_2O	N/A
In_2O Full Coverage Insertion	-1.01 eV/In_2O	-1.12 eV/In_2O
In_2O Half Coverage Over Dimers	-1.26 eV/In_2O	N/A
In_2O Full Coverage Over Dimers	-1.24 eV/In_2O	-1.26 eV/In_2O
In_2O Half Coverage Between Dimers	-0.86 eV/In_2O	N/A
In_2O Full Coverage Between Dimers	Unknown	-0.86 eV/In_2O
Ga_2O Half Coverage Insertion	-1.87 eV/Ga_2O	N/A
Ga_2O Full Coverage Insertion	-1.79 eV/Ga_2O	-1.86 eV/Ga_2O
Ga_2O Half Coverage Over Dimers	-1.06 eV/Ga_2O	N/A
Ga_2O Full Coverage Over Dimers	-1.04 eV/Ga_2O	-1.05 eV/Ga_2O
Ga_2O Half Coverage Between Dimers	-0.69 eV/Ga_2O	N/A
Ga_2O Full Coverage Between Dimers	Unknown	-0.79 eV/Ga_2O

Grayed box denote pinned structures

Calculations were performed on three different bonding sites for both In_2O and Ga_2O existing on both the row and on the trough. The "row insertion site" is formed when an oxide molecule inserts into the As row dimers. Two different trough sites were also examined: the "trough over dimer" site which forms when an oxide molecule bonds to the group III atom at the trough edge, forming a bridge over an As trough dimer, and the "trough between dimer" site which forms when an oxide molecule bonds to the group III molecule at the trough edge, forming a bridge between the As trough dimers.

The enthalpies of adsorption for the In_2O bonding sites on $In_{0.37}Ga_{0.63}As$(001)-(2×4) are presented in Fig. 3(a). The row insertion site and the trough over dimer site are essentially degenerate in energy. Therefore, it is reasonable to assume that In_2O molecules will occupy both the row insertion and the trough over dimer sites, even at low coverage.

For $In_2O/In_{0.37}Ga_{0.63}As$(001)-(2×4), the significant difference in adsorption energies between the two trough sites is most likely a result of dissimilar local environments. An In_2O molecule that bonds between trough As dimers has an unfavorable interaction with the filled dangling bonds on the trough As dimers, while the oxide molecule that bonds over a trough As dimer will experience no such unfavorable interactions. This difference results in the trough between dimer site being less energetically favorable than the trough over dimer site.

Figure 3(b) gives the enthalpies of adsorption for the Ga_2O bonding sites on $In_{0.37}Ga_{0.63}As(001)$-(2×4). Although one might expect Ga_2O and In_2O adsorption energies to be nearly the same, they actually exhibit major differences. The Ga_2O row insertion site is significantly more stable than the In_2O row insertion site (-1.86 eV/Ga_2O *vs.* -1.12 eV/In_2O, respectively). The Ga_2O row insertion site is also significantly more stable than any of the other Ga_2O bonding geometries on $In_{0.37}Ga_{0.63}As(001)$-(2×4). Therefore, at low coverage, only the Ga_2O row insertion sites are expected to form on $In_{0.37}Ga_{0.63}As(001)$-(2×4). The difference in Ga_2O and In_2O stability on InGaAs(001)-(2×4) results from the stronger Ga-As bonds forming a more stable row insertion site than the weaker In-As bonds similar to that seen for the GaAs(001)-(2×4) surface (23).

The calculated $Ga_2O/In_{0.37}Ga_{0.63}As(001)$-(2×4) enthalpies of adsorption clearly indicate that the most favorable bonding geometry is the row insertion site. The differences in adsorption energies between the $Ga_2O/In_{0.37}Ga_{0.63}As(001)$-(2×4) bonding geometries are attributed to three causes. First, Ga-As bonds are stronger than Ga-Ga bonds, causing the row site to be more stable than the trough sites (23). Second, the row site forms four new bonds, while the trough sites only form two, which causes the row site to be more stable than the trough sites. Third, as with In_2O bonding to $In_{0.37}Ga_{0.63}As(001)$-(2×4), unfavorable interaction exists between the filled dangling bonds on the trough As dimer and the trough between dimer site.

Although no experiments have been performed to verify the In_2O or the Ga_2O bonding sites on $In_{0.37}Ga_{0.63}As(001)$-*c*(2×8)/(2×4), the computational modeling results can be compared to the experimentally observed binding sites for In_2O and Ga_2O on GaAs(001)-*c*(2×8)/(2×4). STM imaging results reveal that In_2O bonds to both the row and the trough regions on GaAs(001)-*c*(2×8)/(2×4) at low coverage. Conversely, Ga_2O is found to only bonds on the row on GaAs(001)-*c*(2×8)/(2×4) at low coverage. These results are consistent with the computational findings for In_2O and Ga_2O on $In_{0.37}Ga_{0.63}As(001)$-(2×4).

Density of states and projected density of states calculations

Previous DOS calculations for In_2O and Ga_2O on GaAs(001)-(2×4) were performed on a double slab (i.e. a supercell consisting of two surface unit cells put) (23). This geometry allowed for both half coverage (every other site filled in) and full coverage (every site filled in) adsorption to be considered. In the current study, only one unit cell was simulated, therefore, only full coverage results were obtained. Previous studies found that none of the half coverage sites on GaAs(001)-(2×4) induced significant state density in the band gap but as the coverage increased, states were found to have formed in the band gap region for both In_2O and Ga_2O bonded to GaAs(001)-(2×4), consistent with Fermi level pinning (23). However, none of the high coverage calculated sites were ever seen experimentally for Ga_2O on GaAs(001)-(2×4).

Figure 4(a) shows the DOS for the three different In_2O bonding sites. Of the three sites considered, only one site introduces states into the band gap (row insertion site). As the coverage of In_2O molecules is increased complete trough coverage (every possible trough site filled, utilizing both types of trough sites), the density of states induced in the band gap region also increases [Fig. 4(b)].

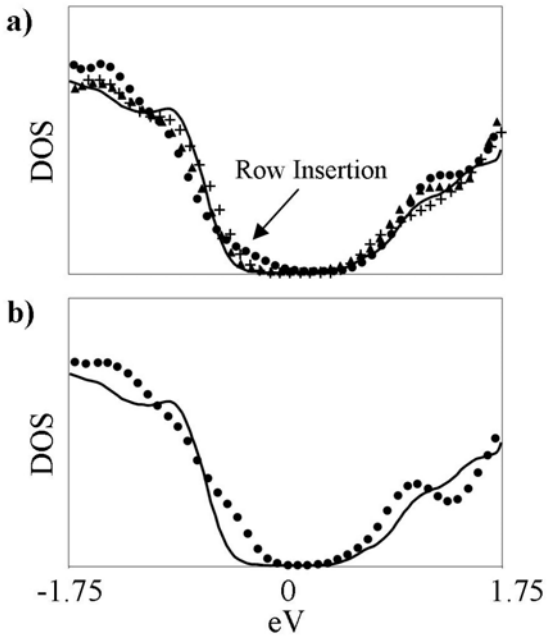

FIGURE 4. (a) Calculated DOS of the single In_2O bonding sites on $In_{0.37}Ga_{0.63}As(001)$-(2×4): clean surface (black solid line), row insertion site (●), trough over dimer (▲), and trough between dimer (+) sites. (b) Calculated DOS of the clean surface (black solid line) and a surface with the trough completely filled in with In_2O molecules (●).

The DOS results for In_2O on $In_{0.37}Ga_{0.63}As(001)$-(2×4) can be compared to the DOS results for In_2O on GaAs(001)-(2×4). For In_2O on GaAs(001)-(2×4), the full coverage insertion and full coverage over dimer sites both possessed states within the band gap, with the largest density of states generated by the full coverage row insertion site (23). Conversely, when In_2O bonds onto $In_{0.37}Ga_{0.63}As(001)$-(2×4) at low coverages, the only site that generates states in the band gap is the row insertion site. These calculations suggest that Fermi level pinning should be less severe for In_2O bonding to $In_{0.37}Ga_{0.63}As(001)$-(2×4) than for In_2O bonding to GaAs(001)-(2×4). When In_2O bonds to either $In_{0.37}Ga_{0.63}As(001)$-(2×4) or GaAs(001)-(2×4), it induces states near the band edges. Because InGaAs has a smaller band gap than GaAs, these In_2O induced states will most likely reside beyond the band edges, but reside between the band edges for GaAs. However, as the In_2O coverage increases the number of states also increases causing the states to eventually arise within the InGaAs band gap.

Figure 5(a) shows the DOS for the three different Ga_2O bonding geometries on $In_{0.37}Ga_{0.63}As(001)$-(2×4). The only low-coverage site that causes state formation in the band gap is the trough between dimer site. The calculated $Ga_2O/In_{0.37}Ga_{0.63}As(001)$-(2×4) sites are comparable to full coverage sites for Ga_2O/GaAs(001)-(2×4), which possess densities of states consistent with Fermi level pinning for both the row full coverage insertion and the trough full coverage over dimer sites (23).

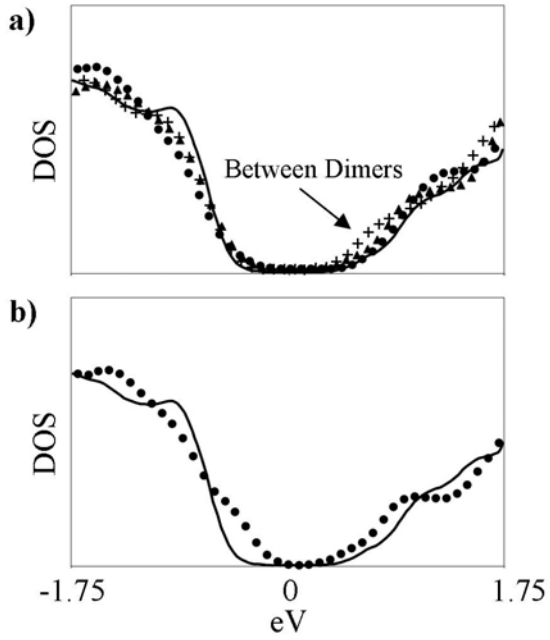

FIGURE 5. (a) Calculated DOS of the single Ga_2O bonding sites on $In_{0.37}Ga_{0.63}As(001)$-(2×4): clean surface (black solid line), row insertion (●), trough over dimer (▲), and trough between dimer (+) sites. (b) Calculated DOS of the clean surface (black solid line) and a surface with the trough completely filled in with Ga_2O (●).

If the Ga_2O concentration is increased to complete trough coverage by the adsorption of Ga_2O molecules onto every available trough site (filling in all between and over dimer sites) on $In_{0.37}Ga_{0.63}As(001)$-(2×4), the apparent Fermi level pinning worsens [Fig. 5(b)] similar to coverage effect found on GaAs (23). However, a greater Ga_2O coverage is needed on InGaAs than on GaAs before Fermi level pinning is observed. InGaAs has a smaller band gap than GaAs, therefore, some of the states that are seen when Ga_2O bonds with GaAs(001)-(2×4) are located outside the band gap region for the InGaAs band gap.

Conclusion

DFT computational simulations of In_2O and Ga_2O bonding to $In_{0.37}Ga_{0.63}As(001)$-(2×4) were performed. Although the adsorption energies are nearly the same for In_2O and Ga_2O adsorbing onto $In_{0.37}Ga_{0.63}As(001)$-(2×4) or GaAs(001)-(2×4), the calculated electronic structures differ slightly. In both cases, increasing the density of oxide molecules increases the density of states in the band gap. However, the number of states in the band gap was smaller for the oxides on $In_{0.37}Ga_{0.63}As(001)$-(2×4) than on GaAs(001)-(2×4). In_2O and Ga_2O induced states were mainly located at the band edges. The InGaAs band gap is smaller than the GaAs band gap causing a significant portion of the pinning states to be located beyond the valence and conduction band edges for InGaAs. This suggests that, in general, forming an unpinned oxide interface on narrow band gap semiconductors may be easier than on wide gap semiconductors. It also suggests that the presence of disorder in the placement of atoms in ternary semiconductors has little effect on the atomic and electronic structure of the interface when the atoms are chemically similar (e.g. Ga and In as opposed to Ga and Al).

Acknowledgments

This work was funded by Intel/UCDiscovery (SPS 97-12.006), the NSF (NSF-DMR--0315794), and the SRC (1437)

References

1. C.B. DeMelo, D.C. Hall, G.L. Snider, D. Xu, G. Kramer and N. El-Zein. *Electronics Letters*, **36**, 84, (2000).
2. F. Ren, J.M. Kuo, M. Hong, W.S. Hobson, J.R. Lothian, J. Lin, H.S. Tsai, J.P. Mannaerts, J. Kwo, S.N.G. Chu, Y.K. Chen and A.Y. Cho. *IEEE Electron Device Letters*, **19**, 309, (1998).
3. P.D. Ye, G.D. Wilk, B. Yang, J. Kwo, H.J.L. Gossmann, M. Hong, K.K. Ng and J. Bude. *Applied Physics Letters*, **84**, 434, (2004).
4. J.M. Millunchick, A. Riposan, B. Dall, C. Pearson and B.G. Orr. *Surface Science*, **550**, 1, (2004).
5. L. Li, B.K. Han, R.F. Hicks, H. Yoon and M.S. Goorsky. *Ultramicroscopy*, **73**, 229, (1998).
6. J.M. Millunchick, A. Riposan, B.J. Dall, C. Pearson and B.G. Orr. *Applied Physics Letters*, **83**, 1361, (2003).
7. A. Chakrabarti, P. Kratzer and M. Scheffler. *Physical Review B*, **74**, (2006).
8. A. Chakrabarti and K. Kunc. *Physical Review B*, **68**, (2003).
9. A. Chakrabarti and K. Kunc. *Physical Review B*, **70**, (2004).
10. J.H. Cho, S.B. Zhang and A. Zunger. *Physical Review Letters*, **84**, 3654, (2000).
11. P. Kratzer, E. Penev and M. Scheffler. *Applied Surface Science*, **216**, 436, (2003).
12. E. Penev, S. Stojkovic, P. Kratzer and M. Scheffler. *Physical Review B*, **69**, (2004).
13. G. Kresse, *VASP*. 1993, Technische University at Wien.
14. G. Kresse and J. Furthmüller. *Computational Materials Science*, **6**, 15, (1996).
15. G. Kresse and J. Furthmüller. *Physical Review B*, **54**, 11169, (1996).
16. G. Kresse and J. Hafner. *Physical Review B*, **47**, 558, (1993).
17. J.P. Perdew, K. Burke and M. Ernzerhof. *Physical Review Letters*, **77**, 3865, (1996).
18. G. Kresse and J. Hafner. *Journal of Physics: Condensed Matter*, **6**, 8245, (1994).
19. D. Vanderbilt. *Physical Review B*, **41**, 7892, (1990).
20. H.J. Monkhorst and J.D. Pack. *Physical Review B*, **13**, 5188, (1976).
21. D.L. Winn, M.J. Hale, T.J. Grassman, A.C. Kummel, R. Droopad and M. Passlack. *Journal of Chemical Physics*, **126**, (2007).
22. J.M. Moison, C. Guille, F. Houzay, F. Barthe and M. Vanrompay. *Physical Review B*, **40**, 6149, (1989).
23. D.L. Winn, M.J. Hale, T.J. Grassman, J.Z. Sexton, A.C. Kummel, R. Droopad and M. Passlack. *Journal of Chemical Physics*, (Submitted).